Interfacial structure, bonding and composition of InAs and GaSb thin films determined using coherent Bragg rod analysis

C. N. Cionca,[1,*] D. A. Walko,[2] Y. Yacoby,[3] C. Dorin,[4,†] J. Mirecki Millunchick,[4] and R. Clarke[1]
[1]*Applied Physics Program, Physics Department, University of Michigan, Ann Arbor, Michigan 48109, USA*
[2]*Advanced Photon Source, Argonne National Laboratory, Argonne, Illinois 60439, USA*
[3]*Racah Institute of Physics, Hebrew University, Jerusalem 91904, Israel*
[4]*Materials Science and Engineering Department, University of Michigan, Ann Arbor, Michigan 48109, USA*
(Received 22 October 2006; published 8 March 2007)

We have used Bragg rod x-ray diffraction combined with a direct method of phase retrieval to extract atomic resolution electron-density maps of a complementary series of heteroepitaxial III-V semiconductor samples. From the three-dimensional electron-density maps we derive the monolayer spacings, the chemical compositions, and the characteristics of the bonding for all atomic planes in the film and across the film-substrate interface. InAs films grown on GaSb(001) under two different As conditions (using dimer or tetramer forms) both showed conformal roughness and mixed GaAs/InSb interfacial bonding character. The As tetramer conditions favored InSb bonding at the interface while, in the case of the dimer, the percentages corresponding to GaAs and InSb bonding were equal within the experimental error. The GaSb film grown on InAs(001) displayed significant In and As interdiffusion and had a relatively large fraction of GaAs-like bonds at the interface.

DOI: 10.1103/PhysRevB.75.115306 PACS number(s): 68.03.Hj, 68.35.Fx, 68.55.−a, 81.15.−z

I. INTRODUCTION

Heteroepitaxial materials based on compound semiconductors have emerged as a major driver of optoelectronics technology. An extremely important aspect of this development is the quest for materials suitable for infrared applications such as detectors, imagers, and sources.[1] From the large family of III-V materials, InAs and GaSb share several interesting properties from the device engineering point of view. They both exhibit direct, narrow band gaps (at room temperature E_{InAs}=0.36 eV and E_{GaSb}=0.72 eV), making them attractive candidates for infrared lasers and detectors.

Both InAs and GaSb have zinc-blende structure; their lattice constants are similar (~0.6% mismatch) allowing high values of the critical thickness and thus creating the possibility of building devices with high efficiency. However, the epitaxial growth of semiconductor heterostructures containing these materials proved to be difficult because of the miscibility in the quaternary alloy InGaAsSb,[2] and the strong segregation tendencies of both In and Sb. Several theoretical studies have implied that such compositional effects, and the characteristics of the bonding at the film-substrate interface, have an important bearing on the electronic properties of these materials.[3–7] For example, In and Sb segregation can lead to a blueshift of the band gap.[3]

A first step toward controlling the electronic behavior in these materials is to understand the morphology of the film-substrate interface. This still proves to be a challenging task because only a few experimental techniques can be used to investigate buried interfaces. Since intermixing is significant, knowledge of the actual chemical composition and bonding across the interface is important. To address this question, cross-section scanning tunneling microscopy (XSTM) studies have been reported.[8–10] Based on these results, the segregation energies could be determined using the kinetic model of Dehaese *et al.*[11]

Although it is a very powerful technique, XSTM has a few significant limitations. The scans can only be done in the directions corresponding to the cleavage planes and thus not all atomic planes can be imaged. Only those atomic layers corresponding to a specific crystallographic cleavage plane through the sample can be investigated. Since atomic resolution is needed in this type of XSTM scan, only a limited area can be probed.

Compared to scanning probe microscopy, x-ray scattering has several important advantages: it can probe all the atomic planes in the film-substrate system, the method is nondestructive, a larger sample area can be evaluated and, most important, it can probe buried interfaces. In this study, we used a recently developed x-ray phase reconstruction technique, coherent Bragg rod analysis (COBRA),[12] which is especially useful for studying epitaxial thin films. The method provides three-dimensional electron density (ED) maps of the structure with sub-Å resolution throughout the film and the near-interface region of the substrate. From these results, the out-of-plane lattice spacing, the chemical composition, and the bond distribution were extracted in a layer-by-layer fashion as a function of position. The method does not require detailed prior knowledge of the system structure, nor is it based on a fit refinement procedure in which the parameters are defined *a priori*.

II. SAMPLE PREPARATION

All samples were grown in a molecular-beam epitaxy chamber equipped with solid sources for Ga and In and valved cracking cells for As and Sb. The interfacial bonding was intended to be InSb-like for all samples by controlling the shutter opening sequence. The flux of each element was calibrated by observing reflection high energy electron diffraction (RHEED) oscillations on appropriate substrates using a KSA 400 data acquisition system.

A. InAs thin films grown on GaSb substrates

Two samples of InAs were grown on GaSb (001) substrates. We will refer to these samples as InAs(4) and InAs(2). For sample InAs(2), the temperature of the cracker cell was set at $t_{As}=1000$ °C, corresponding to an As flux rich in As(2) dimers. Sample InAs(4) was grown with the cracker temperature set at $t_{As}=600$ °C, which promotes a molecular flux rich in As(4) tetramers.

The substrate temperature was set to $t_{subs}=530$ °C as calibrated using an optical pyrometer. Prior to growth, the surface was maintained in a partial pressure of Sb of $\sim 5 \times 10^{-7}$ Torr. The desorption of the native oxide layer was monitored by observing the RHEED pattern. Once diffraction spots appeared, the substrate temperature was quickly ramped down to $t_{subs}=360$ °C, and a 0.3-μm-thick homoepitaxial GaSb buffer layer was grown, group V terminated. The InAs film was deposited by migration enhanced epitaxy (MEE).[13] That is, a single atomic layer (AL) of In is deposited on GaSb, followed, after a predetermined delay of a few seconds, by a single AL of As. This scheme was employed in an attempt to promote the formation of an InSb interfacial layer, which has been shown to result in higher quality detectors.[14] In total, nine monolayers (MLs) of InAs were grown, where one ML of InAs consists of one AL of In and one AL of As.

B. GaSb grown on InAs substrates

The InAs substrate was maintained at approximately $t_{subs}=520$ °C until the change in the RHEED pattern indicated that the oxide was desorbed. A 0.2-μm InAs buffer layer was deposited at a substrate temperature of $t_{subs}=460$ °C and the substrate temperature was then ramped down to $t_{subs}=360$ °C. MEE was also used for this sample in an attempt to influence the interface bonding. In this case, a single AL of Sb was deposited on In-terminated InAs, followed by a single AL of Ga. The procedure is designed to result in an InSb interface. In total, nine MLs of GaSb were deposited during which RHEED intensity oscillations were observed, suggesting a layer-by-layer growth mode.

III. BRAGG ROD MEASUREMENTS

A. Experimental setup

The x-ray-scattering pattern of a bulk crystal consists of Bragg peaks and its surface termination induces an additional diffuse scattering pattern along lines normal to the surface, referred to as *Bragg rods* or *crystal truncation rods*.[15] The intensity along the Bragg rods is much smaller than that of the bulk Bragg peaks, commonly by 8–10 orders of magnitude; nevertheless, the intensity profile along the Bragg rods contains detailed information about the structure of the termination surface. In the case of an epitaxial film, the Bragg rod profiles also can be used to determine the atomic structure of the film and the interface.

The x-ray studies were performed at the MHATT-XOR beamline at sector 7 of the Advanced Photon Source. The x rays were produced by an undulator insertion device and the desired energy was selected using a Si⟨111⟩ double-crystal monochromator situated 30m downstream from the insertion device. The monochromated beam was conditioned both horizontally and vertically with two sets of slits and was focused vertically using a Rh coated Si mirror. The focusing point was positioned in the center of the goniometer, 55 m downstream from the undulator. After conditioning, the beam size was ~ 400 μm horizontally by 50 μm vertically. We used a six-circle diffractometer operating in Eulerian geometry.

The x-ray detector consisted of a plastic scintillator in front of a Hamamatsu RG47-04 photomultiplier tube with a low-noise preamplifier. To meet the requirements for a high dynamic range imposed by the signal intensity along the rods, the detector was operated in dc mode (as a current amplifier). To access the maximum range of Bragg rods while avoiding background counts from x-ray fluorescence, an x-ray energy of 10.25 keV was chosen.

Because the incident beam fluence was $>10^{12}$ s^{-1}, attenuators had to be used to extend the dynamic range of the detector. They consisted of a bank of Cu foils of thicknesses 10, 20, 40, and 80 μm and they were only used in the vicinity of the Bragg points. Spectral contamination by higher harmonic x rays was reduced by setting the incident angle of the focusing mirror to be well above the critical angle for the total external reflection by third-harmonic x rays but below that for the first order x rays. A software package developed for Bragg rod acquisition by Yacoby *et al.*[16] was used to control the diffractometer and to facilitate the data acquisition.

B. Data acquisition

Throughout this paper we define the x, y, and z directions of the sample to be along the ⟨100⟩ axes, with x and y in the surface plane and z perpendicular to the surface. The corresponding reciprocal-lattice coordinates, given in reciprocal-space units of the sample substrate, are h, k, and L, respectively.

For every sample, seven Bragg reflections were used to find the orientation matrix. The substrate miscut was small enough not to induce significant splitting in the Bragg rods. Data were acquired along hKL rods with indices in the range $|h|, |k| \leq 4$, and $L \leq 5.5$, with integer h, k either odd-odd or even-even and L positive and continuously varying. The mixed index rods (even-odd) were not measured as the structure factor of the zinc-blende structure cancels out in this case. Rods $00L$, $11L$, $20L$, $22L$, $31L$, $33L$, $40L$, $42L$, and $44L$ were measured with a data density of 100 points for every reciprocal lattice unit (RLU).

To perform the Fourier transforms associated with the direct method (see below), symmetry equivalent rods were generated using the $p2mm$ plane group symmetry. The sample (001) axis was set in the vertical plane containing the incident beam. For the symmetric $00L$ rod, the angles between the incident and diffracted beams with the (001) plane were equal. For the rest of the rods, the angle formed between the incident beam and the (001) plane was set to $\sim 3.5°$. Given the size of the beam defined above, its footprint on the sample at this angle of incidence was ~ 400 μm

horizontally by ~800 μm in the direction of the beam. At every point along the rod a background intensity was also measured. Since the incident beam was polarized in the horizontal plane, the background-subtracted intensities were corrected for polarization and Lorentz factor effects.[17,18]

IV. DATA ANALYSIS

A. Coherent Bragg rod analysis

The goal of the COBRA phase retrieval method is to obtain the complex structure factor (CSF) along the experimentally measured Bragg rods. Once this is achieved, the electron density is obtained as the result of an inverse three-dimensional Fourier transform. In a scattering experiment, only the magnitude of the complex structure factor can be immediately obtained from the scattered intensity. Structure factors can be transformed into the electron density of the sample, but only if the real and imaginary components of the CSF are known. This is the classic problem of phase determination in x-ray crystallography. To retrieve the total CSF of the sample, we first create a virtual structure built with nominal parameters of the system, such as total thickness, approximate crystallographic structure, composition, and roughness. We refer to the structure factor of this virtual structure as the *reference*. The difference between the total and reference structure factors then is the *unknown* structure factor. The modulus of this unknown structure factor can be determined if the intensity profile is measured along the Bragg rod with a high sampling density, based on the fact that the CSF varies continuously along the rods. The method has been discussed in detail in Refs. 12 and 19 and generally is applicable to systems which are periodic in two dimensions and are coherent with respect to the substrate. This is the situation corresponding to pseudomorphic epitaxial heterostructures and encompasses many materials of importance to electronic materials technology.

The structure factor was extracted only in a finite region of the reciprocal space, centered at the origin. To calculate the CSF in all quadrants, symmetry operations specific to the plane symmetry group were used. The boundaries of this finite volume were correlated with the ones dictated by the experiment. The upper limit of measurement was chosen to be L_{max}=5.5, which minimized data truncation artifacts. For every sample, the phasing routine was applied three times successively to obtain the final result.

Finally, the three-dimensional (3D) electron density is obtained as an inverse Fourier transform of the CSF. Figure 1 is an example of a [110] section through the ED of sample GaSb, representing the upper part of the InAs substrate and the GaSb film. Because of the the symmetry of the zinc-blende structure, a [110] plane section intersects only half of the atoms in the unit cells investigated. To have access to all atoms in the unit cell, two plane sections are needed. Since the full three-dimensional density is now determined, another section can be taken to include the other half of the atoms. This is a considerable advantage over the XSTM technique in which only the exposed surface plane is accessible.

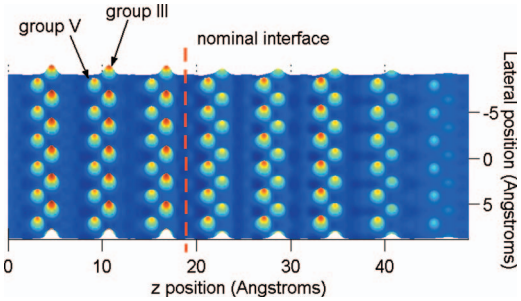

FIG. 1. (Color) [110] cross section of the 3D electron density through the film-substrate interface for the GaSb sample; only two of every four atoms are visible in this particular plane cross section. The position of the nominal interface is shown by the dashed line.

The quality of the ED obtained in this way was checked by comparing the experimental diffraction intensities with the diffraction intensities calculated from the COBRA-derived EDs. Figure 2 displays the measured data and the diffraction intensity profile calculated from the COBRA-derived electron density for one of the nine measured rods (31L). The two are in good agreement. However, the final result is not perfect mainly because real samples can have some mosaicity or other types of irregularity which tend to smear the interference conditions. This level of agreement

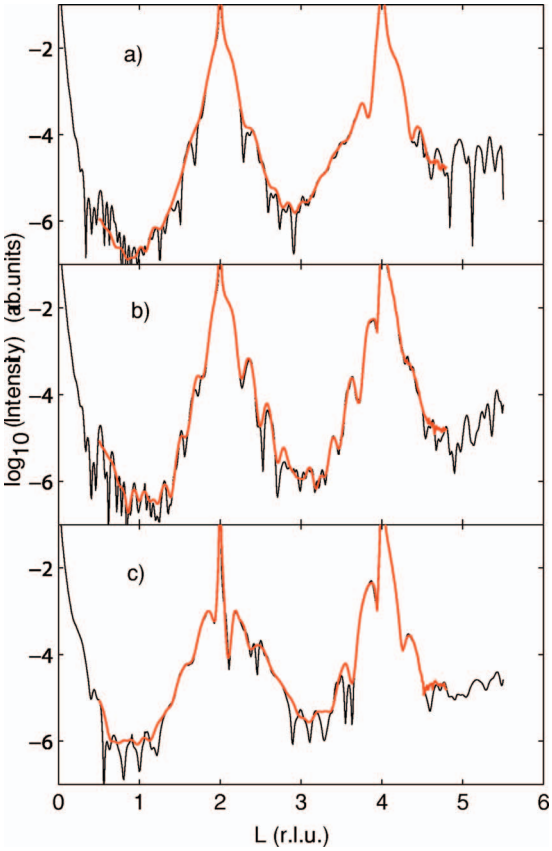

FIG. 2. (Color) Measured 31L rods (red) and COBRA-derived intensity profile (black) for (a) sample InAs(4), (b) sample InAs(2), and (c) sample GaSb. The vertical scale was truncated to emphasize the features along rods; on this scale, the Bragg points would occur around +2.

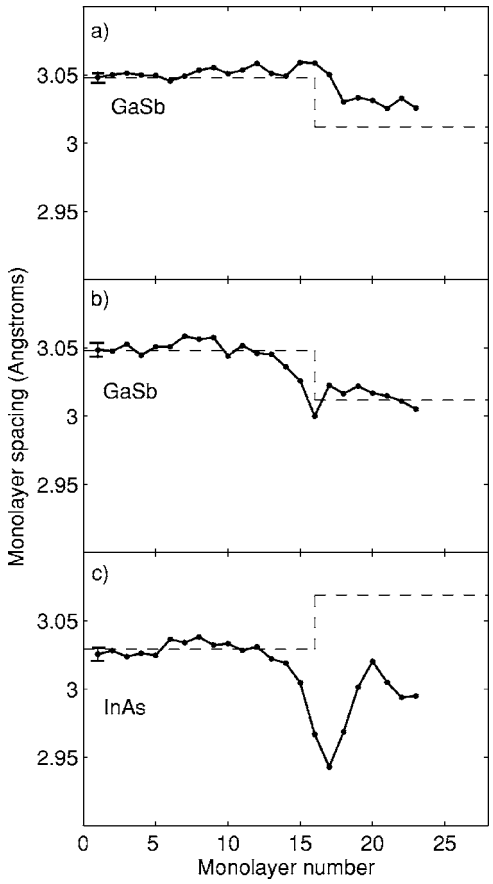

FIG. 3. Monolayer spacing for (a) sample InAs(4), (b) sample InAs(2), (c) sample GaSb; solid line: experimental data; dashed line: nominal value of the monolayer spacing, corresponding to an ideal substrate and coherently strained film. The corresponding uncertainties (σ) are represented by the error bars.

was obtained for all Bragg rods and all three samples measured in this study, demonstrating that the COBRA routine is able to successfully phase the CSF in each case.

B. Extracting the chemical composition

Obtaining the 3D electron density is only the first step of the analysis. From the electron density we can obtain a great deal of useful information, not only about the structure, but also its chemical composition and bonding characteristics. Typically the lattice parameters are used to infer compositional information (e.g., through Vegard's law). Here we take a self-consistent approach to extract the chemical composition and bonding information. We fit the ED of the film to peaks whose positions and integrated intensities A yield the spacing between monolayers (Fig. 3) and the effective number of electrons at a given atomic position, respectively.

The whole volume of the film and near-substrate region will be regarded as a quaternary alloy, $Ga_mIn_{1-m}Sb_nAs_{1-n}$ with $m=m(z)$ and $n=n(z)$ having a functional dependence on vertical position z and m,n both satisfying $0 \leqslant m,\ n \leqslant 1$. A general assumption for the quaternary alloy is that intermixing will occur only between same-group atoms, i.e., between group-III atoms (In, Ga) and group-V atoms (As, Sb) so that the possibility of antisite defects is neglected. For every point along z the compositional fractions $m(z)$ and $n(z)$ need to be determined to fully describe the average chemical composition of the film and its interface with the substrate.

The quaternary composition of the alloy implies that every peak in the ED contains a contribution of two terms:

$$m(z) \cdot Z_{\mathrm{Ga}} + [1 - m(z)] \cdot Z_{\mathrm{In}} = A_{III}(z) \tag{1}$$

and

$$n(z) \cdot Z_{\mathrm{As}} + [1 - n(z)] \cdot Z_{\mathrm{Sb}} = A_V(z). \tag{2}$$

$Z_{\mathrm{Ga}}=26.34$, $Z_{\mathrm{In}}=49.06$, $Z_{\mathrm{As}}=31.27$, and $Z_{\mathrm{Sb}}=51.06$ are the effective numbers of electrons for the corresponding atoms at the energy of 10.250 keV;[20] A_{III} and A_V are the integrated ED peaks corresponding to the group-III and group-V atoms, respectively. Equations (1) and (2) can be applied in the region of the film where the fractional occupancy is close to unity. This includes the most important region of the system we are interested in, namely the film-substrate interface. For this reason, the chemical composition was not calculated for the top one or two monolayers of the film, where surface roughness significantly decreased the layer's total electron density. Since the values of electron density are known up to a multiplicative factor, the values for A_{III} and A_V have to be normalized. For both group-III and group-V sites, the normalization constant was determined as the ratio between the corresponding Z values of the chemical constituents and the integrated ED peaks in the substrate region, far from the interface.

Solving Eqs. 1 and 2 yields the values of m and n for every monolayer throughout the film and and heterointerface region. Figure 4 displays the values of m (group-III composition) and n (group-V composition) as a function of vertical position for all three samples considered in this paper.

V. EXTRACTING THE BONDING AT THE HETEROINTERFACE

The COBRA method has unique advantages in probing the type of chemical bonding that forms the interface (i.e., whether we have InSb-like bonds or GaAs-like bonds and how much of each). This is crucial information towards understanding the electronic behavior of epitaxial materials and devices, essentially in controlling the growth to achieve desirable electronic characteristics.

We calculated the bonding distribution (fraction of each kind of bond) using an approach based on the composition fractions m,n and the values of the monolayer spacing presented in Fig. 3. Assuming no antisite defects, four possible types of bonds can be present at a given height z, with probabilities x_{GaSb}, x_{GaAs}, x_{InSb}, and x_{InAs} satisfying

$$x_{\mathrm{GaSb}}(z) + x_{\mathrm{GaAs}}(z) + x_{\mathrm{InSb}}(z) + x_{\mathrm{InAs}}(z) = 1, \tag{3}$$

$$x_{\mathrm{GaSb}}(z) + x_{\mathrm{GaAs}}(z) = m(z), \tag{4}$$

$$x_{\mathrm{GaSb}}(z) + x_{\mathrm{InSb}}(z) = n(z). \tag{5}$$

Since the film is coherent with the substrate the unit cell will, in general, be tetragonally distorted. In order to be able

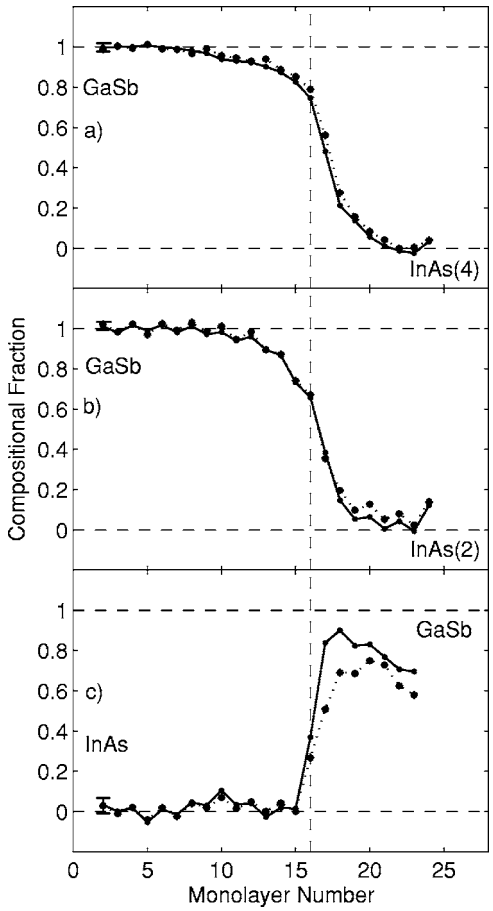

FIG. 4. Chemical composition of (a) sample InAs(4), (b) sample InAs(2) and (c) sample GaSb; $m(z)$: solid line, the average group-III composition. $m=1$ corresponds to pure Ga and $m=0$ to pure In; $n(z)$: dotted line, the average group-V composition. $n=1$ corresponds to pure Sb and $n=0$ to pure As. The vertical dashed line is the position of the nominal interface. The error bar corresponds to one standard deviation, σ.

to use Vegard's law, the measured values of the vertical lattice parameter were corrected for biaxial strain using the expression

$$a_c(z) = \frac{a_{subs} + a_{ED}(z)p}{1+p}, \tag{6}$$

where a_{subs} is the lattice parameter of the substrate, $a_{ED}(z)$ is the vertical lattice parameter extracted from the ED as twice the monolayer spacing, $p=\frac{2\nu}{1-\nu}$ (ν is the Poisson ratio), and $a_c(z)$ is the corresponding cubic lattice parameter, which is subsequently used in Vegard's law:

$$x_{\mathrm{GaSb}}(z)a_{\mathrm{GaSb}} + x_{\mathrm{GaAs}}(z)a_{\mathrm{GaAs}} + x_{\mathrm{InSb}}(z)a_{\mathrm{InSb}} + x_{\mathrm{GaSb}}(z)a_{\mathrm{InAs}} = a_c(z), \tag{7}$$

where the bulk lattice parameters of the binary compounds are $a_{\mathrm{GaAs}}=5.6533$ Å, $a_{\mathrm{InAs}}=6.0584$ Å, $a_{\mathrm{GaSb}}=6.0959$ Å, and $a_{\mathrm{InSb}}=6.4794$ Å.

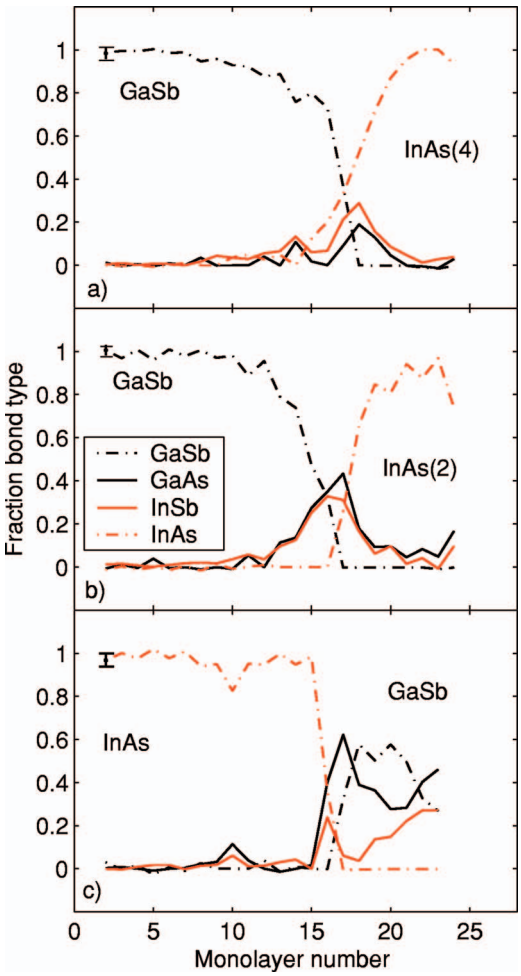

FIG. 5. (Color) The bonding distribution for (a) sample InAs(4), (b) sample InAs(2), (c) sample GaSb; black dashed line: percentage GaSb bonds; black solid line: percentage GaAs bonds; red solid line: percentage InSb bonds; red dashed line: percentage InAs bonds. The corresponding σ error bar was plotted for the first point of every sample.

Solving Eqs. (3)–(5) and (7) yields the values of the probabilities for all possible bonds in every monolayer in the considered region, as displayed in Fig. 5.

VI. RESULTS AND DISCUSSION

The behavior of the InAs films grown on GaSb substrates is quite similar in both samples. The In and As contents vary as expected: zero in the GaSb substrate, increasing in the interfacial region and becoming close to unity in the InAs film. An error function fit of the chemical composition profile yielded a standard deviation value of $\sigma=12.7$ Å for the sample grown under As(4) overpressure and $\sigma=13.9$ Å for the sample grown using As(2). The composition fractions $m(z)$ and $n(z)$ track each other remarkably well in both InAs(4) and InAs(2) samples [Figs. 4(a) and 4(b)], with the proviso that sample InAs(2) has a slightly wider transition region between film and substrate. The fact that the group-III and group-V composition fractions follow each other closely

is indicative of an interface morphology comprised of biatomic height steps and conformal roughness. If instead the interfaces were broadened by interdiffusion, the profiles for the different species would not follow each other closely due to different segregation rates. The bonding distribution profiles [Figs. 5(a) and 5(b)] show that the bonding has mixed InSb and GaAs character in both cases. It appears that InSb bonds are favored somewhat ($\sim 3:2$ ratio) over GaAs bonding when the InAs films are grown in an As(4) atmosphere. On the other hand, for an As(2) atmosphere, the ratio of InSb to GaAs bonding is, within the experimental error, $\sim 1:1$. The small dip in the monolayer spacing [Fig. 3(b)] at the nominal position of the interface in the case of sample InAs(2) also points toward the increased preference for GaAs bonding noted above, taking into account the fact that the GaAs bond length is considerably smaller than any of the other possibilities in this quaternary system. The content of GaAs-like bonds in this case is probably due to the higher reactivity of As(2) relative to As(4). In the case of InAs(4) [Fig. 3(a)] the dip is absent indicating an interface structure with a smaller percentage of GaAs bonds.

In the case of GaSb films grown on InAs substrates the monolayer spacing never reaches the value corresponding to coherently strained GaSb. In addition to that, the decrease in the value of monolayer spacing in the vicinity of the nominal interface is much more prominent than in the case of sample InAs(2), as seen in Fig. 3(c). The lattice strain in the vertical direction is nonuniform and relatively large ($\sim 2\%$).

The interface is significantly more abrupt for the GaSb film on the InAs substrate compared to the case of InAs on GaSb, presumably due to a smoother initial surface. The results show that for GaSb on InAs the behavior of the chemical composition [Fig. 4(c)] is significantly different than for the case of InAs films on GaSb substrates: the film never reaches the stoichiometry corresponding to GaSb. Also, the composition fractions $m(z)$ and $n(z)$ do not follow each other as in the case of InAs films, indicating that segregation takes place at the substrate-film interface. The composition fractions indicate that there is a significant amount of In and As in the GaSb film. The origin of the As is possibly due to residual arsenic vapor pressure in the growth chamber. The high content of In ($\sim 30\%$) can be explained given its tendency to surface segregate.[11,21,22] The bonding distribution in the film and across the interface confirms the presence of As, participating mostly in GaAs-type of bonds [Fig. 5(c)]. InSb-type bonding seems to be present towards the surface of the film, again indicating a tendency of In to segregate towards the surface.

VII. CONCLUSIONS

We have demonstrated that the COBRA method is a very powerful direct probe of structure and chemical bonding in heteroepitaxial electronic materials. It is unique in being able to provide atomic scale resolution information on the structure and chemical composition of the interfaces as well as the nature and distribution of the interface bonding. The element specificity was achieved without resorting to resonant scattering techniques. The amount of detail in the electron density provides extremely valuable feedback to growers who are interested in tuning the deposition parameters to optimize the structure and obtain specific types of bonding at the interfaces. The generality of the approach described here shows that it can be useful for a wide variety of epitaxial heterostructures including superlattices, atomic layer structures, quantum dot arrays, and quantum wires.

ACKNOWLEDGMENTS

This work was conducted at the MHATT-XOR beamline at the Advanced Photon Source and was supported in part by the U.S. Department of Energy, Grant No. DE-FG01-06ER46273 and National Science Foundation, Grant No. DMR-0606048. Use of the Advanced Photon Source was supported by the U.S. Department of Energy, Office of Science, Office of Basic Energy Sciences, under Contract No. DE-AC02-06CH11357.

*Electronic address: codrin@umich.edu
†Presently at Intel Corp.

[1] J. Singh, *Electronic and Optoelectronic Properties of Semiconductor Structures* (Cambridge University Press, Cambridge, United Kingdom, 2003).
[2] G. B. Stringfellow and P. E. Greene, J. Phys. Chem. Solids **30**, 1779 (1969).
[3] R. Magri and A. Zunger, Phys. Rev. B **65**, 165302 (2002).
[4] R. Magri and A. Zunger, Phys. Rev. B **68**, 155329 (2003).
[5] W. H. Lau and M. E. Flatte, Appl. Phys. Lett. **80**, 1683 (2002).
[6] R. Magri and A. Zunger, IEE Proc.-J: Optoelectron. **150**, 409 (2003).
[7] D. H. Chow, R. H. Miles, and A. T. Hunter, J. Vac. Sci. Technol. B **10**, 888 (1992).
[8] R. M. Feenstra, D. A. Collins, and T. C. McGill, Superlattices Microstruct. **15**, 215 (1994).
[9] B. Z. Nosho, W. Barvosa-Carter, M. J. Yang, B. R. Bennet, and L. J. Whitman, Surf. Sci. **465**, 361 (2000).
[10] J. Steinshnider, J. Harper, M. Weimer, C. H. Lin, S. S. Pei, and D. H. Chow, Phys. Rev. Lett. **85**, 4562 (2000).
[11] O. Dehaese, X. Wallart, and F. Mollot, Appl. Phys. Lett. **71**, 52 (1995).
[12] Y. Yacoby, R. Pindak, R. MacHarrie, L. Pfeiffer, L. Berman, and R. Clarke, J. Phys.: Condens. Matter **12**, 3929 (2001).
[13] Y. Horikoshi, M. Kawashima, and H. Yamaguchi, Jpn. J. Appl. Phys., Part 2 **25**, L868 (1986).
[14] M. S. Daly, D. M. Symons, M. Lakrimi, R. J. Nicholas, N. J. Mason, and P. J. Walker, Semicond. Sci. Technol. **11**, 823 (1996).
[15] I. K. Robinson and D. J. Tweet, Rep. Prog. Phys. **55**, 599 (1992).
[16] Y. Yacoby, D. A. Walko, M. Sowwan, R. Clarke, R. Pindak, R. MacHarrie, J. Pitney, E. Stern, and D. Brewe, in *Synchrotron*

Radiation Instrumentation, edited by T. Warwick, J. Arthur, H. A. Padmore, and J. Stöhr, AIP Conf. Proc. No. 705 (AIP, Melville, NY, 2004), pp. 1221–1224.
[17] M. Sowwan, Ph.D. thesis, Hebrew University, 2002.
[18] E. Vlieg, J. Appl. Crystallogr. **30**, 532 (1997).
[19] M. Sowwan, Y. Yacoby, J. Pitney, R. MacHarrie, M. Hong, J. Cross, D. A. Walko, R. Clarke, R. Pindak, and E. A. Stern, Phys. Rev. B **66**, 205311 (2002).
[20] B. L. Henke, E. M. Gullison, and J. C. Davis, At. Data Nucl. Data Tables **54**, 181 (1993).
[21] J. F. Zheng, J. D. Walker, M. B. Salmeron, and E. R. Weber, Phys. Rev. Lett. **72**, 2414 (1994).
[22] C. Renard, X. Marcadet, J. Massies, I. Prevot, R. Bissaro, and P. Galtier, J. Cryst. Growth **259**, 69 (2003).